Dark Matter as Cantor Dust: Numerical Evidence

Ervin Goldfain

Global Institute for Research, Education and Scholarship (GIRES), USA

E-mail ervingoldfain@gmail.com

Abstract

As benchmark model of complex dynamics, Stuart-Landau (SL) equation describes the universal behavior of nonlinear oscillators near a Hopf bifurcation. The bifurcation gives birth to a stable, finite-amplitude periodic motion called a *limit cycle*. Here we develop a one-dimensional toy model showing how Dark Matter (DM) follows from the SL equation. We outline how fluctuations in the control parameter $\mu(x)$ of the SL equation generate progressive amplitude fragmentation, a process mimicking the iterative construction of Cantor sets. The emerging structure freezes in a cosmological phase known as *Cantor Dust*, a spontaneously broken condensate whose effective dimension flows from 1 to a non-integer $D<1$. The resulting fractal dimension computed numerically ($D\approx 0.9$) reinforces the hypothesis of running spacetime dimensions near the Planck scale.

Key words: complex dynamics, complex Ginzburg-Landau equation, Stuart-Landau equation, Cantor Dust, continuous dimensions, dimensional flow.

1. Introduction

It has been known for quite some time that large-scale cosmic structures exhibits hallmarks of *multifractal dynamics*, including clustering across scales, lacunarity, and long-range correlations [1-2, 11-14]. These properties suggest that standard continuous-density models may be insufficient to capture the grainy and self-similar organization recorded in astrophysical data.

A promising alternative arises from nonlinear amplitude equations such as the Complex Ginzburg–Landau Equation (CGLE) and its reduced case, the Stuart–Landau (SL) equation, both being considered universal models of nonlinear dynamics. Building off [17-19], here we adopt the hypothesis that dimensional fluctuations of deep ultraviolet physics can be adequately modeled by amplitude fields obeying the SL equation. Fluctuations in the driving parameters of this equation lead to *progressive amplitude*

fragmentation, which replicates the iterative construction of Cantor sets. Developing this insight, we provide numerical evidence that the dynamic behavior of the SL equation, under fluctuations of its control parameter μ(x), generates *Cantor Dust*, a spontaneously broken condensate whose effective dimension flows from 1 to a non-integer $D<1$. When μ(x) fluctuates about zero, localized regions effectively approach Hopf instability, forming oscillatory patches that progressively break up into multifractal dust-like sets. The resulting fractal dimension computed numerically ($D\approx 0.9$) supports the conjecture that spacetime dimensions are continuous entities running with the probing energy scale near the Planck regime. In this picture, DM is the result of *dimensional condensation*, a process forming relic cosmological structures left over from the primordial Universe.

2. Theoretical background

The complex amplitude field A (x, t) of CGLE and SL equations evolves under the influence of the control parameter μ(x), which regulates the local

departure to oscillatory instability. Spatial fluctuations of $\mu(x)$ arise naturally from background inhomogeneities, noise, or coupling to additional fields.

Regions where $\mu(x)$ is locally suppressed toward zero behave as if close to Hopf bifurcation. Here, oscillatory modes grow, interact, and fragment, producing primordial structures—spatial patterns with partial coherence. Continued modulation leads to *Cantor-Dust–like* fragmentation characterized by lacunarity, self-similarity, and reduced fractal dimension.

The local fractal dimension $D(x)$ serves as a diagnostic of fragmentation, and departures from a uniform distribution are measured by

$$\varepsilon(x) = 1 - D(x) \ll 1$$

As $\mu(x)$ drives deeper fragmentation, $D(x)$ drops below 1 and epsilon(x) increases, reflecting progressive fragmentation. Such multifractal distributions naturally mimic DM by creating gravitational potentials consistent with observations, without invoking new particles [see e.g., 20]. Thus CGLE/SL dynamics driven by spatially fluctuating $\mu(x)$ offers a

physically motivated mechanism for the formation of DM mass distributions.

3. Starting point: CGLE with spatial inhomogeneity

We begin with the spatially extended CGLE [3-4]:

$$\partial_t A(x,t) = (\mu(x) + i\omega_0)A - (1 + ic_2) \mid A \mid^2 A + (1 + ic_1)\, \partial_x^2 A + \eta(x),$$

where the control parameter $\mu(x)$ exhibits quenched spatial fluctuations around a mean value μ_0, and $\eta(x)$ represents small-amplitude noise. Neglecting the gradient term in the weak-coupling limit gives the local SL dynamics:

$$\partial_t A(x,t) = (\mu(x) + i\omega_0)A - (1 + ic_2) \mid A \mid^2 A.$$

In the context of this work, the amplitude field |A(x)| takes on the role of *dimensional density*. Writing the amplitude–phase representation $A = Re^{i\theta}$ yields the coupled partial differential equations:

$$\partial_t R = \mu(x)R - R^3,$$

$$\partial_t \theta = \omega_0 - c_2 R^2.$$

The amplitude dynamics decouples from θ, and the fixed points of R are:

$$R = 0;\ R = \sqrt{\mu(x)}.$$

Thus, the *local physical amplitude* is uniquely determined by $\mu(x)$. The spatial field $\mu(x)$ breaks up into alternating regions of:

- $\mu(x) < 0$: amplitude collapses $R(x) \to 0$, producing *voids*.
- $\mu(x) > 0$: finite-amplitude oscillations occur, producing *peaks.*

Iterating this fragmentation reproduces the prescription "remove–keep–remove" in the recursive construction of Cantor sets (Fig. 1). Numerical experiments show that the empirical mapping is well modeled by the exponential map:

$$\epsilon(x) = \epsilon_0(1 - e^{-\alpha\mu(x)}),$$

a monotonic relation consistent with higher oscillatory activity corresponding to smaller effective dimensions $D(x)$.

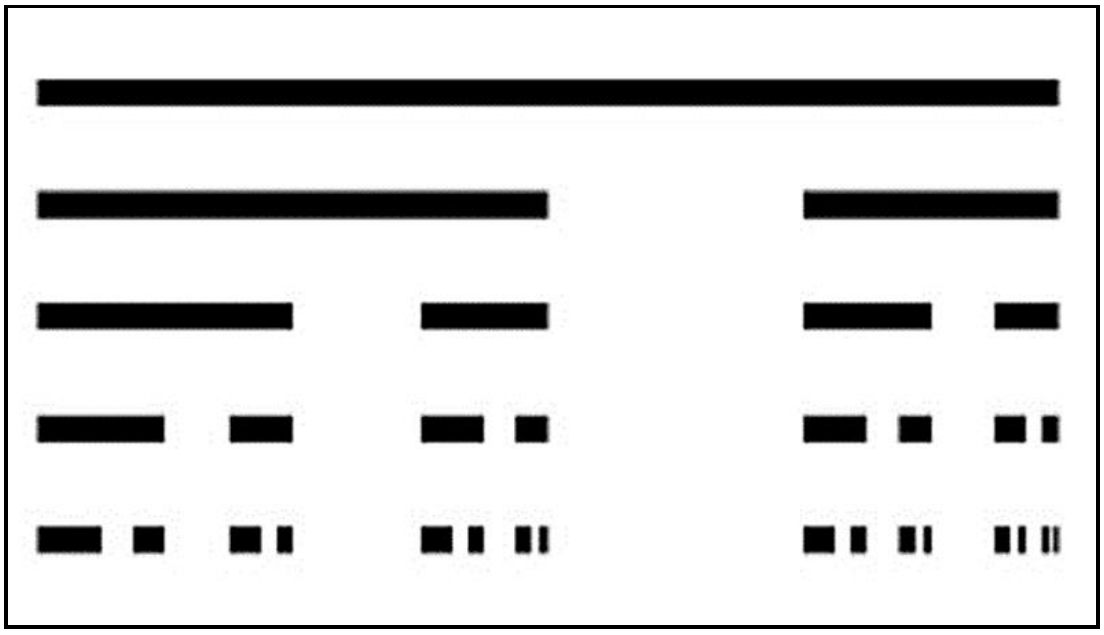

Fig. 1: Recursive construction of a two-scale Cantor set

Given the sampled field $\mu(x)$ and computed amplitudes $R(x)$, we proceed in several steps,

1. Normalize $\mu(x)$ to the unit interval.
2. Apply the exponential map to compute the dimensional deviation $\epsilon(x)$.
3. Obtain the effective dimension via $D(x) = 1 - \epsilon(x)$. This yields direct maps of local effective geometry.

4. Numerical Results

4.1 Amplitude snapshots

High-resolution amplitude profiles $R(x)$ show increased fragmentation as regions with negative $\mu(x)$ collapse to zero while positive patches form isolated peaks. As previously mentioned, this reflects the iterative formation of Cantor Dust in the theory of Cantor Sets.

4.2 Box-counting dimension and dimensional maps

Applying a standard box-counting algorithm to the thresholded set yields a log–log slope (box counting dimension):

$$D_{\text{eff}} \approx 0.90$$

This lies below unity and matches the expected dimension for a nonideal, noisy Cantor-like set. Figs. 4 and 5 show the following.

- $\epsilon(x)$ displays sharp spikes at fragmentation sites.

- $D(x)$ exhibits complementary voids, indicating local geometric collapse.

Maps of ε(x) and D(x) were computed by two complementary mappings (see paragraph 6. 3 below).

4.3 Phase portraits and histogram

Figs. 6 and 7 of local phase portraits (R, θ) reveal clustering around the limit-cycle radius $R = \sqrt{\mu(x)}$. As expected, regions with $\mu(x) < 0$ collapse to the origin, while regions with $\mu(x) > 0$ form annular clusters. This provides another dynamic confirmation of the fragmentation mechanism. Fig. 7 displays the phase histogram as number of counts versus phase.

5. Details on the numerical simulation.

- 1D CGLE was integrated on Python code, with a spatially varying control parameter $\mu(x)$.
- Domain: $\mathrm{L} = 256$, $\mathrm{N} = 2048$ grid points, periodic boundaries.

- Time increment dt = 0.02, t_{MAX} = 120, c_1 = 1.0, c_2 = 1.5, mean $\mu_0 = -0.1$ and scaled by $\mu_{\text{sigma}} = 0.6$.
- Noise added as small additive Gaussian term with amplitude η =0.02.

6. Simulation results

6.1 Final amplitude | $A(x)$ |

- Computed as $|A(x)| = \sqrt{Re(A)^2 + Im(A)^2}$. When plotted vs x. shows intertwined islands of peaks and voids.

6.2 Box-counting dimension

- Covered domain with boxes of sizes $b = 2^n$ (in grid points) up to $N/8$.
- Counted boxes containing any occupied point; plotted $\log N(\epsilon)$ vs $\log(1/\epsilon)$ and fitted a line over the scaling range.
- Estimated global effective dimension $D \approx 0.9022$ for the run; Recall that the value of the box-counting dimension varies with input parameters, seed and threshold.

6.3 Local $\varepsilon(x)$ and $D(x)$ maps and complex plane scatter

Two separate techniques were deployed, namely,

- **Amplitude-based mapping**: for data points sampled across the domain, local mass $m(\ell; x) = \int_{B_\ell(x)} | A |^2 \, dx$ was computed at multiple scales ℓ, fitted as $\log m(\ell)$ vs. $\log \ell$ to get the local slope $D(x)$. Interpolation was extended to the full grid and local dimensional deviation computed as $\varepsilon(x) = 1 - D(x)$.
- **Probabilistic mapping**: coarse-grained values of the control parameter $\mu_r(x)$ and a Gaussian distribution were assumed in order to estimate survival probability $p(x) = P(\mu_r > \mu_c)$; probability $p = (1/s)^\varepsilon$ was inverted with $s = 1/3$ to obtain $\varepsilon(x)$ and $D(x) = 1 - \varepsilon(x)$. Both mappings were plotted for comparison.
- Complex-plane scatter: *Re(A)* vs *Im(A)* shows annular clusters where oscillations persist and points near origin where amplitude collapsed. High density sampling was used for enhanced visualization.

6.5 Phase histogram

- Phase $\phi(x) = \arg(A(x))$.
- Phase vs x: shows phase coherence within peaks and phase gaps at boundaries.

Below are the representative plots discussed above.

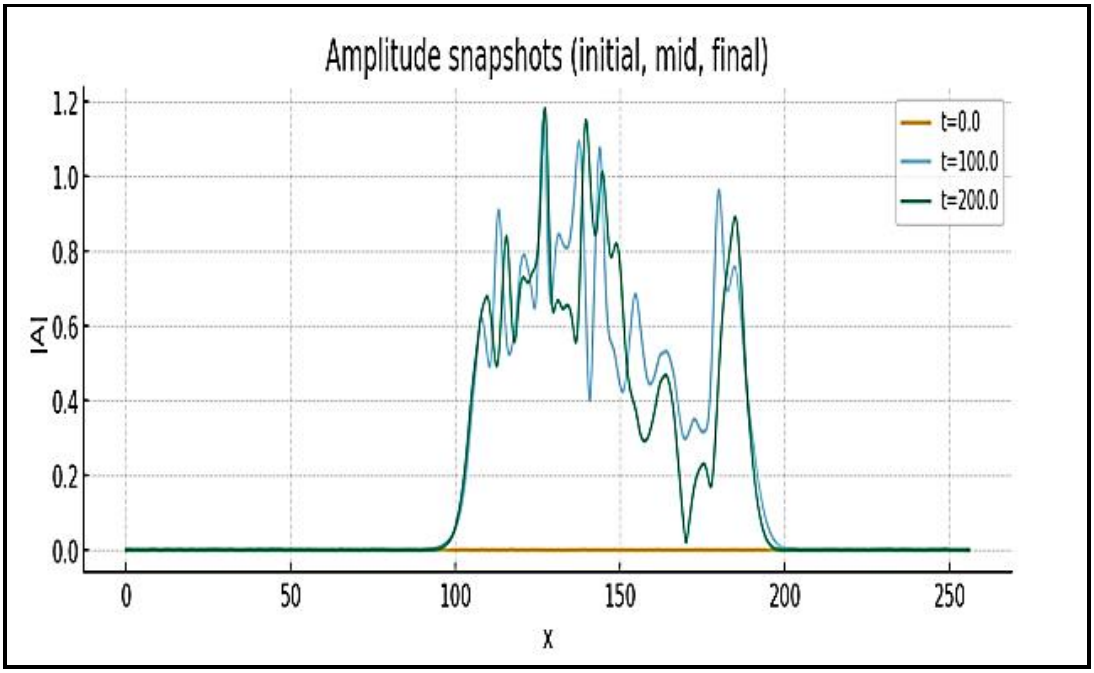

Fig 2: Snapshots showing progressive amplitude fragmentation.

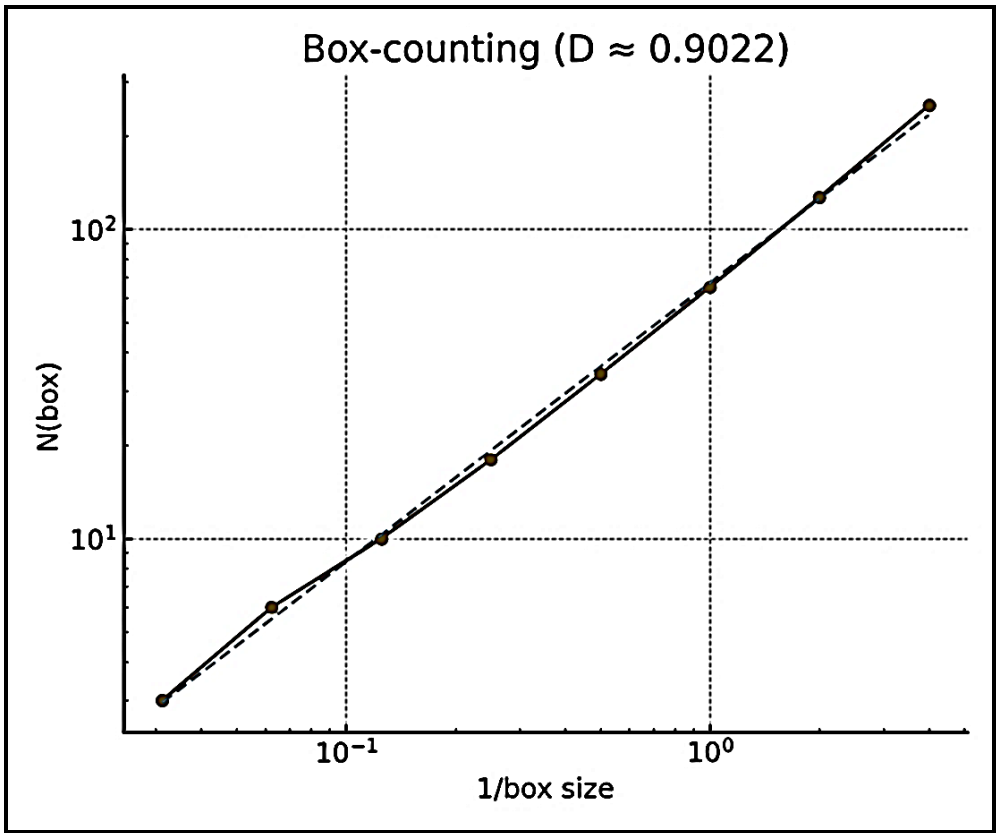

Fig 3: Box-counting log–log plot. Estimated global D ≈ 0.9022.

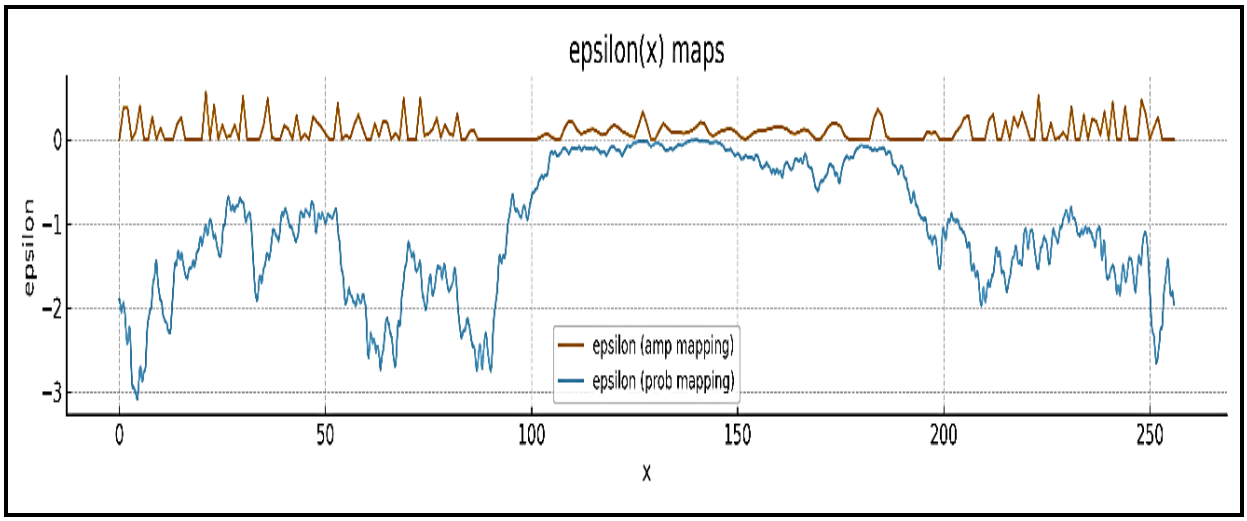

Fig 4: ε(x) maps (amplitude-based and probabilistic mappings).

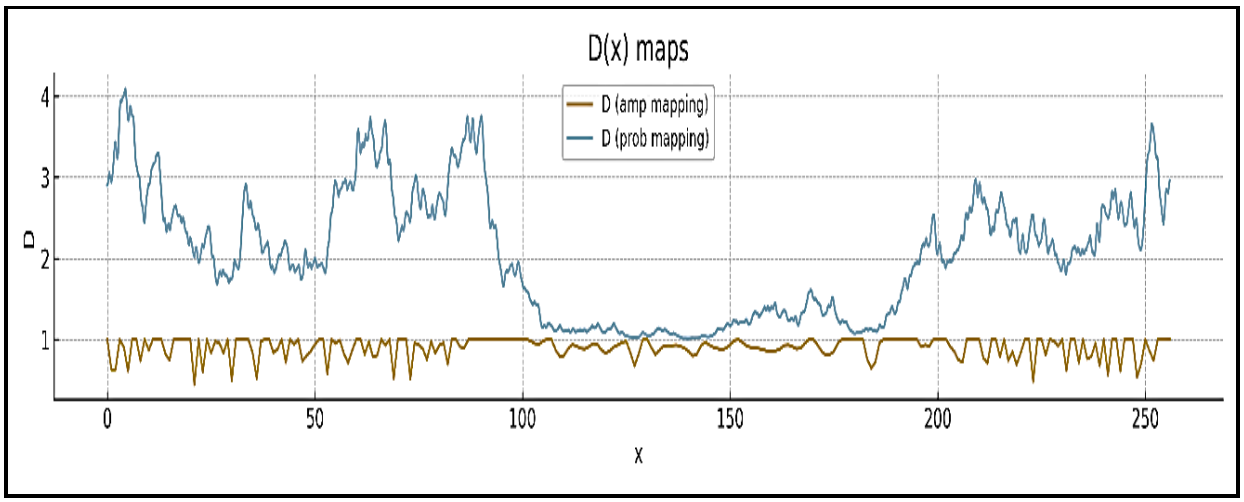

Fig. 5: D(x) maps (amplitude-based and probabilistic mappings).

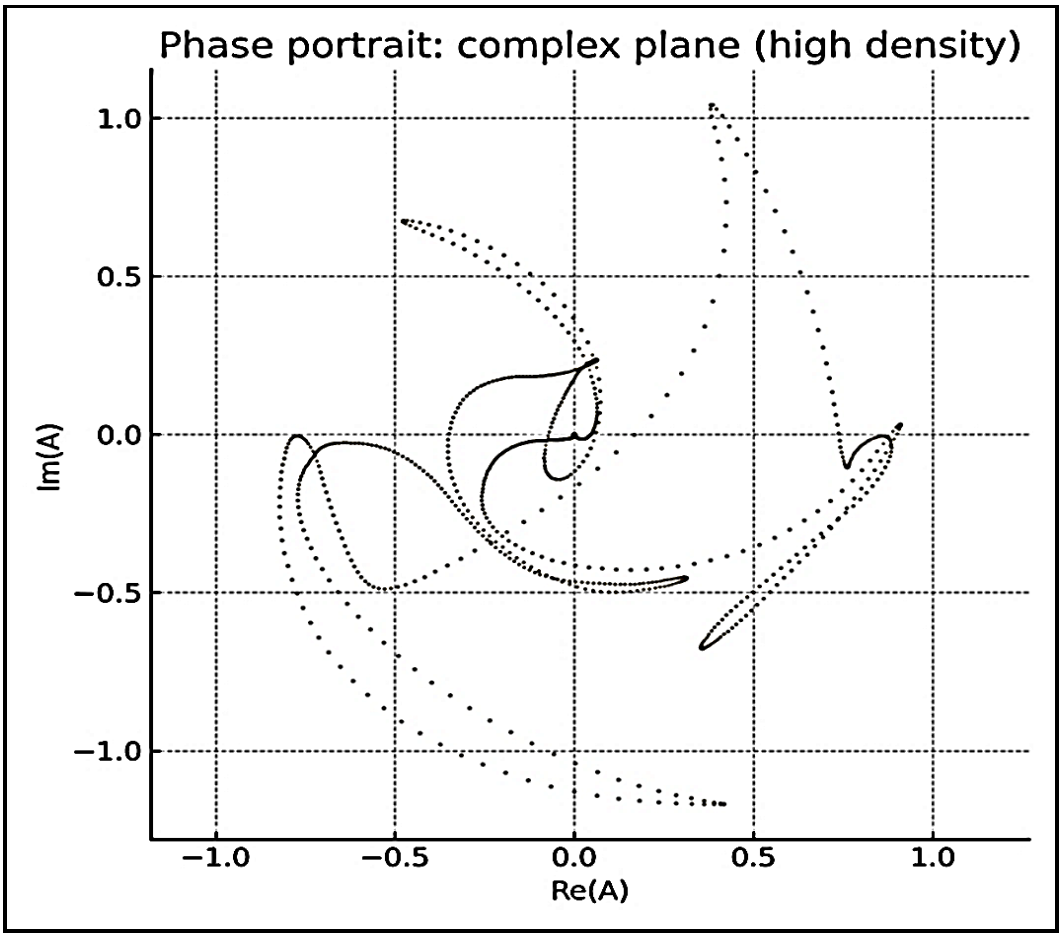

Fig. 6: Phase portrait (complex plane scatter)

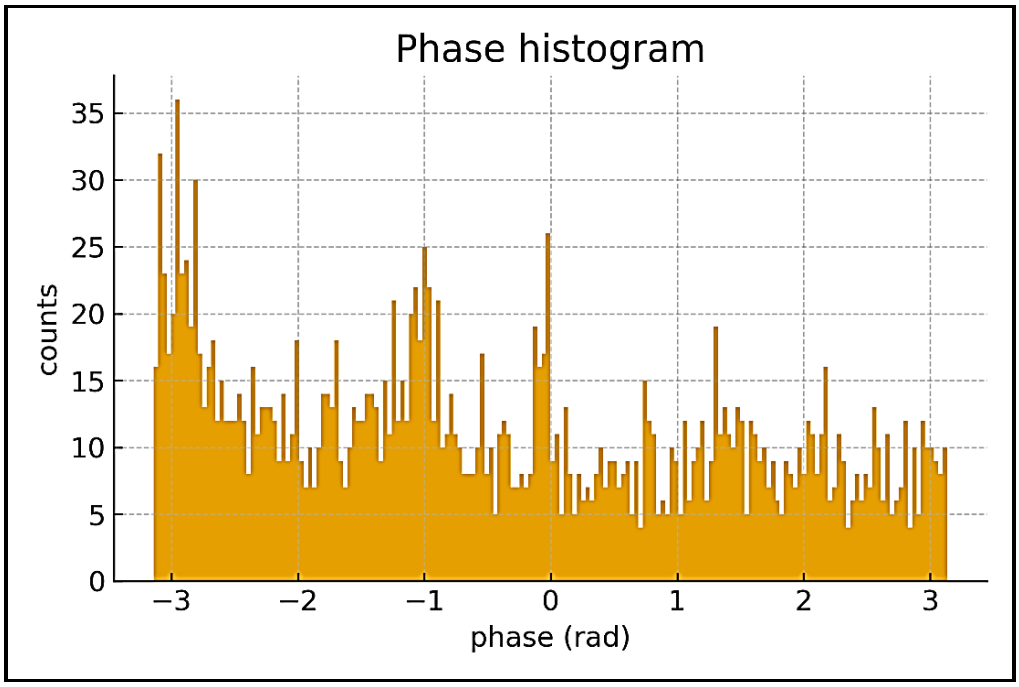

Fig 7: Phase histogram

7. Concluding remarks

Both CGLE and SL equations provide a natural mechanism for the emergence of Cantor Dust from scale-induced fluctuations of $\mu(x)$. The SL scenario backs up the idea of *multifractal geometry* of primordial spacetime, in which continuous dimensions condense into cosmological structures. Numerical simulations corroborate the theory, producing a fractal dimension near $D \approx 0.90$.

In a nutshell, numerical evidence shown here suggests that,

- DM is the result of a dimensional condensation process,
- This process generates multifractal structures compatible with the formation of Cantor Dusto.

Future work may include 2D/3D CGLE simulations, multifractal spectra, a links to fractional dynamics governing the evolution of matter fields in the early Universe and to the study of topological defects and topological condensation [1].

We close with a word of caution: a possible objection to this work is that it is based on a *circular argument*: we started from the Reaction-Diffusion (RD) model of continuous dimensional fluctuations, arrived at the CGLE and the SL equations, numerically analyzed them and concluded that it supports the Cantor Dust structure of DM. But this is, in fact, another form taken by the RD model of dimensional fluctuations, which we started with.

The counterargument is that both CGLE and SL equations are not necessarily connected to primordial dimensional fluctuations. They are universal models of nonlinear dynamics and complex behavior [4-10], emerging from the *reduction to normal forms of bifurcation equations in the center manifold theory* [15-16].

References

1. E. Goldfain, (2025), "On Complex Dynamics and Primordial Structure Formation", preprint https://doi.org/10.13140/RG.2.2.32895.32167/1

2. E. Goldfain, (2023), "Cantor Dust and the Gravitational Wave Background", preprint https://doi.org/10.13140/RG.2.2.19323.49447

3. I.S. Aranson & L. Kramer, (2022), "The world of the complex Ginzburg–Landau equation," *Rev. Mod. Phys.* **74**, 99.

4. M.C. Cross & P.C. Hohenberg, (1993), "Pattern formation outside of equilibrium," *Rev. Mod. Phys.* **65**, 851.

5. K. Falconer, (2014), *Fractal Geometry: Mathematical Foundations and Applications*, 3rd ed., Wiley.

6. T. Vicsek, (1992), *Fractal Growth Phenomena*, World Scientific.

7. U. Frisch, (1995), *Turbulence: The Legacy of A.N. Kolmogorov*, Cambridge Univ. Press.

8. B. B. Mandelbrot, (1982), *The Fractal Geometry of Nature*, W. H. Freeman.

9. G. Paladin & A. Vulpiani, (1987), "Anomalous scaling and multifractals in turbulence," *Phys. Rep.* **156**, 147–225.

10. P. Grassberger & I. Procaccia, (1983), "Measuring the strangeness of strange attractors," *Physica D* **9**, 189–208.

11. P. J. E. Peebles, (2020), *Cosmology's Century*, Princeton Univ. Press.

12. M. J. Aschwanden, (2012), "SOC systems in astrophysics", preprint https://arxiv.org/pdf/1207.4413.

13. E. Goldfain, (2024), "Notes on Critical Phenomena and Primordial Cosmology", preprint https://doi.org/10.32388/8Y7NQU.2

14. J. Gaite, (2019), "The Fractal Geometry of the Cosmic Web and Its Formation", preprint https://arxiv.org/pdf/1810.02311

15. G. Nicolis and I. Prigogine, (1977), *Self-organization in Nonequilibrium Systems,* Wiley.

16. J. Guckenheimer and P. Holmes, (1983), *Nonlinear Oscillations, Dynamical Systems and Bifurcations*, Springer.

17. E. Goldfain, (2025), "General Relativity from Primordial Dimensional Fluctuations", preprint https://doi.org/10.13140/RG.2.2.33155.16165/1

18. E. Goldfain, (2025), "Classical Field Theory from Primordial Dimensional Fluctuations", preprint https://doi.org/10.13140/RG.2.2.33971.08483/2

19. E. Goldfain, (2025), "Higgs Mechanism from Primordial Dimensional Fluctuations", preprint https://doi.org/10.13140/RG.2.2.16252.40321

20. E. Goldfain, “Dark Matter as Dimensional Condensate” (2022), preprint

https://doi.org/10.32388/8A8579